Chapter 22
Light-Induced Processes in Porphyrin-Fullerene Systems

Alexander S. Konev

Abstract Porphyrin-fullerene dyads are representative class of donor-acceptor molecular systems capable of undergoing photoinduced charge separation, the phenomenon that is the key process in solar energy conversion systems either in organic solar cells or photoredox catalysis. The charge-separated state generated in covalently linked dyad is a highly polarized electronically excited state. Formation of this state typically proceeds as a result of the relaxation of a locally excited state of higher energy, which is populated upon the initial excitation of the dyad. The review of computational and spectroscopic studies of the excited states in porphyrin-fullerene covalently linked dyads is given in the present chapter.

22.1 Introduction

Donor-acceptor dyads capable of undergoing photoinduced charge separation are useful in both understanding of photoredox processes occurring in the natural photosynthesis and in the design of catalytic systems for artificial photon initiated redox reactions mimicking photosynthesis [1, 2]. Donor-acceptor photoreactive combinations include porphyrins [3], mesytylene [4], carotenoids [5], polythiophens [6] and phtalocyanines [7] as donors and fullerenes C_{60} [3], C_{70} [8], carbon nanotubes [9], acridinium salts [4] and porphyrins [10] as acceptors. Probably the most studied are porphyrin-fullerene dyads and more complicated molecular ensembles bearing porphyrin-fullerene system as the key fragment.

The photoinduced charge separation in porphyrin-fullerene dyads might be used for solar energy harvesting in photoinduced charge-separation type solar cells [3, 11–14]. In particular, Yamada [14] have recently reported superiority of a porphyrin-fullerene covalent dyad over porphyrin-fullerene blend in p-i-n organic photovoltaic

A. S. Konev (✉)

Institute of Chemistry, St. Petersburg State University, Universitetskii pr. 26 Peterhof, St. Petersburg 198504, Russian Federation
e-mail: a.konev@spbu.ru

cells. Recent DFT-based finding that Zn-porphyrin-fullerene dyad should show high rate of an electron transfer to graphene support [15] inspires further studies in this direction.

The ability of porphyrin-fullerene dyads to undergo photoinduced charge separation was well documented in a number of reviews which summarize the experimental achievements of the groups of Sakata [12], Guldi [16], D'Souza [3], Imahori [11, 17], Lemmetyinen [18], Nakamura [19] and Ito [20]. To achieve better understanding of the charge separation phenomenon in porphyrin-fullerene dyads a large number of computational research was reported, the latest review given by Agnihotri [21].

In this chapter, quantum chemical and spectroscopic description of the issues related to the charge separation process in covalently linked porphyrin-fullerene dyads are combined to obtain picture, which reflects both theoretical and experimental data and to provide the reader with the introductory bibliographic guide on the topic.

22.2 Electronic Structure of Porphyrin-Fullerene Dyads

The electronic structure of the ground state of porphyrin-fullerene dyads can be ideally described as consisting of fullerene-localized, porphyrin-localized and mixed molecular orbitals, with HOMO localized on porphyrin and LUMO—on fullerene fragment and charge separated state corresponding to $HOMO^1LUMO^1$ electronic configuration. A representative example of the idealized non-interacting case can be the electronic structure of dyad **1c** (Fig. 22.1) with large separation of the chromophores [22]. Actual degree of mixing of the atomic orbitals belonging to porphyrin or fullerene fragment upon formation of molecular orbitals depends on the geometry of the dyad.

According to the computational study of Zandler and D'Souza [23] at B3LYP/3-21G(*) level of theory, close face-to-face arrangement of the porphyrin and fullerene moieties, where the fullerene spheroid is situated above the center of the porphyrin plane, results in some mixing of the atomic orbitals of the donor and acceptor and endows the charge-transfer character to the ground state in Zn- or Mg-metallated
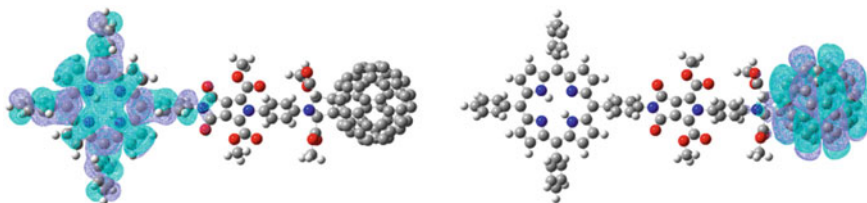

Fig. 22.1 HOMO (left) and LUMO (right) orbitals of dyad **1c** (B3LYP, 6-31G(d,p))

Packman-type porphyrin-fullerene dyads **Zn-2** and **Mg-2** (Fig. 22.2). However, no such interaction was reported for the corresponding free-base dyad **2** (Fig. 22.2). The authors explain this observation by the increased separation between the chromophores in the case of free-base dyad [23].

This is in line with the studies of Lemmetyinen et al. who demonstrated the dependence of the degree of charge transfer on the interchromophore distance. Interchromophore interaction in the ground state was reported for Packman-type porphyrin-fullerene covalent dyad **3a**, where chromophores were connected by a rigid benzanilide-based linker. The interchromophore distance and the charge transfers were found to be 6.3–7.9 Å and 0.09–0.15e respectively depending on the functional used [24]. Shorter interchromophore distance of 5.8 Å (SVWN functional), achieved in a specific conformer of a cyclophane-type dyad **4**, increases the charge-transfer character of the ground state to ca. 0.23e (SVWN functional) [25]. The conformer with larger separation of the chromophores (6.1 Å, SVWN functional) demonstrated lesser degree of charge transfer (0.12e, SVWN functional) [25]. In accord with the observed increase of charge transfer upon decrease of the interchromophore distance is the increased delocalization of HOMO and LUMO over both porphyrin and fullerene systems [25]. In-plane positioning of the porphyrin fragment with respect to the fullerene core (dyad **5**) tends to decrease the degree of charge transfer in the ground state (0.08e, 6.89 Å interchromophore distance, B3LYP functional) [26].

In this connection, a crucial effect of van der Waals corrections on the predicted molecular geometry and, hence, electronic structure, reported in the recent work of Hukka et al. [27] should be mentioned. According to the authors, application of either Grimme [28] or Elstner [29] dispersion correction schemes affects strongly the optimal geometry of porphyrin-fullerene dyad **3b** resulting in delocalization of the HOMO orbital localized on porphyrin moiety for non-corrected structure over the adjacent linker [27].

Experimentally, the interchromophore interaction in the ground state was demonstrated by observing red shift and broadening of the Soret band as compared to the fullerene-free porphyrin [30–34]. In these systems, a new broad absorption feature called charge-transfer (CT) band appears in the near IR, which was initially assigned to the direct population of the charge-separated state from the ground state [35] but was shown later to include formation of exciplex state which has a variable degree of charge transfer [31]. The definition of range for this absorption feature varies from 700–750 nm [30] to 650–750 nm [36] for free-base dyad, from 650–800 nm [31, 35] to 600–1000 nm [32] for Zn-porphyrin-fullerene dyad and from 650–900 to 750–1000 nm for Mg-porphyrin-fullerene dyad [33]. The charge transfer character of the exciplex is evidenced from the red shift of the CT band in the series non-metallated (**4b**), Zn-metallated (**Zn-4b**) and Mg-metallated (**Mg-4b**) dyad, which repeats the order of oxidation potential decrease [36]. In line with this is the observed red shift of the CT band of Zn-metallated dyad **Zn-4a** upon ligation with Cl⁻ or Br⁻ ions due to the stabilization of the polarized exciplex state [37].

Formation of the exciplex state is also confirmed by observation of new emission bands at 730 nm for non-metallated dyad **4b** and at 810 nm [31] (730 nm [38]) for
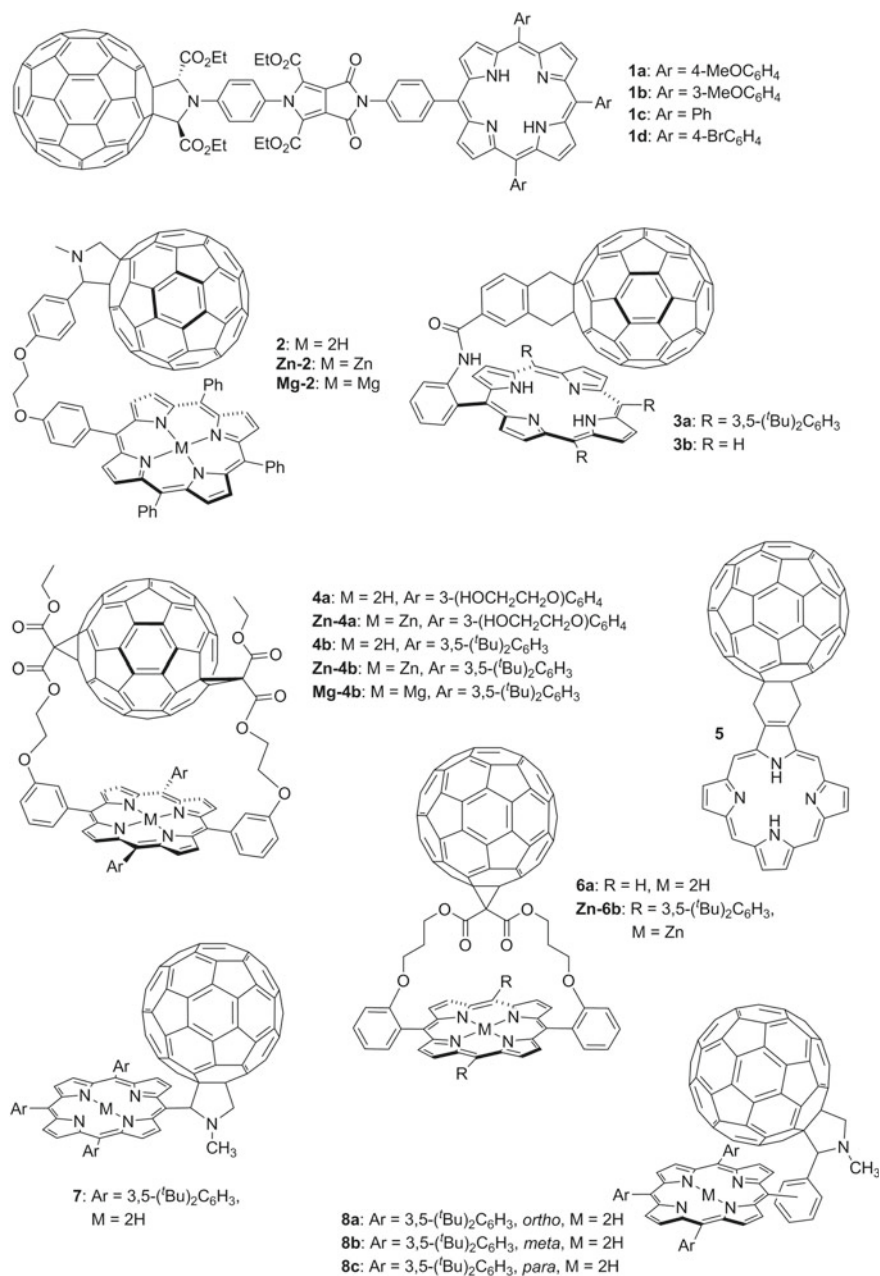
1a: Ar = 4-MeOC$_6$H$_4$
1b: Ar = 3-MeOC$_6$H$_4$
1c: Ar = Ph
1d: Ar = 4-BrC$_6$H$_4$

2: M = 2H
Zn-2: M = Zn
Mg-2: M = Mg

3a: R = 3,5-(^{t}Bu)$_2$C$_6$H$_3$
3b: R = H

4a: M = 2H, Ar = 3-(HOCH$_2$CH$_2$O)C$_6$H$_4$
Zn-4a: M = Zn, Ar = 3-(HOCH$_2$CH$_2$O)C$_6$H$_4$
4b: M = 2H, Ar = 3,5-(^{t}Bu)$_2$C$_6$H$_3$
Zn-4b: M = Zn, Ar = 3,5-(^{t}Bu)$_2$C$_6$H$_3$
Mg-4b: M = Mg, Ar = 3,5-(^{t}Bu)$_2$C$_6$H$_3$

5

6a: R = H, M = 2H
Zn-6b: R = 3,5-(^{t}Bu)$_2$C$_6$H$_3$,
M = Zn

7: Ar = 3,5-(^{t}Bu)$_2$C$_6$H$_3$,
M = 2H

8a: Ar = 3,5-(^{t}Bu)$_2$C$_6$H$_3$, *ortho*, M = 2H
8b: Ar = 3,5-(^{t}Bu)$_2$C$_6$H$_3$, *meta*, M = 2H
8c: Ar = 3,5-(^{t}Bu)$_2$C$_6$H$_3$, *para*, M = 2H

Fig. 22.2 Structural formulae of dyads **1**–**8**

metallated dyad **Zn-4b**. The assignment of this band is in line with the observed strong decrease of the emission intensity, shift of the emission maximum to the red and broadening of the spectral band upon increase of the solvent polarity, characteristic of exciplex-type emission [30, 31].

In accord with the computational results, electronic interaction of the chromophores decreases upon increase in the separation of fullerene and porphyrin moieties. For example, porphyrin-fullerene dyads **6** with parachute topology and large interchromophore distance, show no appreciable electronic interaction of the chromophores in the ground state [39]. The disappearance of the interchromophore interaction was traced in the series of porphyrin-fullerene dyads where porphyrin was attached either directly to fulleropyrrolidine core (**7**, 8.9 Å center-to-center distance) or via ortho- (**8a**, 9.7 Å), meta- (**8b**, 10.9 Å) or para-substituted (**8c**, 12.6 Å) phenyl ring. The red-shift of the Soret band was observed only for dyads with close arrangement of the chromophores (dyads **7** and **8a**) [38].

22.3   Electronically Excited States of Porphyrin-Fullerene Dyads

The TDDFT studies on electronically excited states and the transitions between them for porphyrin-fullerene dyads were reported in a number of works for various dyads.

Qualitative analysis of the computational results shows that the electronically excited states can be classified to (i) states corresponding to local excitation of either porphyrin or fullerene chromophore, which are populated when the electron is excited from an orbital localized on the corresponding chromophore to the orbital localized on the same chromophore, and to (ii) charge transfer states, which are populated when the electron transition occurs between orbitals localized on different chromophores (Fig. 22.3). For example, excitation of an electron from HOMO to LUMO+4 orbital in dyad **1c** can be considered as local excitation of the porphyrin fragment (Fig. 22.4). Similar to the description of the electronic structure, this classification is an ideal case and pure separation between the above types of electronically excited states is not always observed.

For example, Theodorakopoulos et al. report HOMO–LUMO excitation (pure case of charge transfer) to contribute only 68% to the lowest charge-separated state (1.67 eV, B3LYP) in dyad **9** (Fig. 22.5) [40]. An example of the pure case of charge separated state can be found in the work of Krasnov et al. who found the lowest electronically excited state (1.87 eV, oscillator strength 0.02) in dyad **5** to originate solely from HOMO to LUMO excitation [26]. These results agree well with the conclusion of Cramariuc et al. [24] that the contribution of HOMO–LUMO one-electron transition to the charge-separated state depends on the interchromophore distance: the shorter the distance, the larger is the interaction of the chromophores and, hence, the larger is "contamination" of the charge-separated state by local one-electron transitions. An example of well separated local excitations and charge separated states
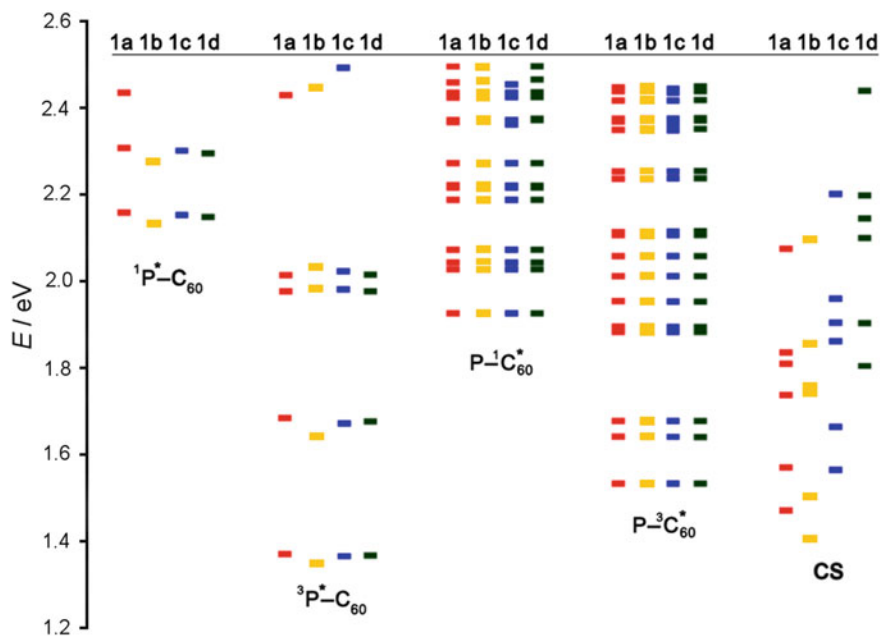
Fig. 22.3 Classification of electronically excited states in dyads **1a–d**. Data taken from [22]
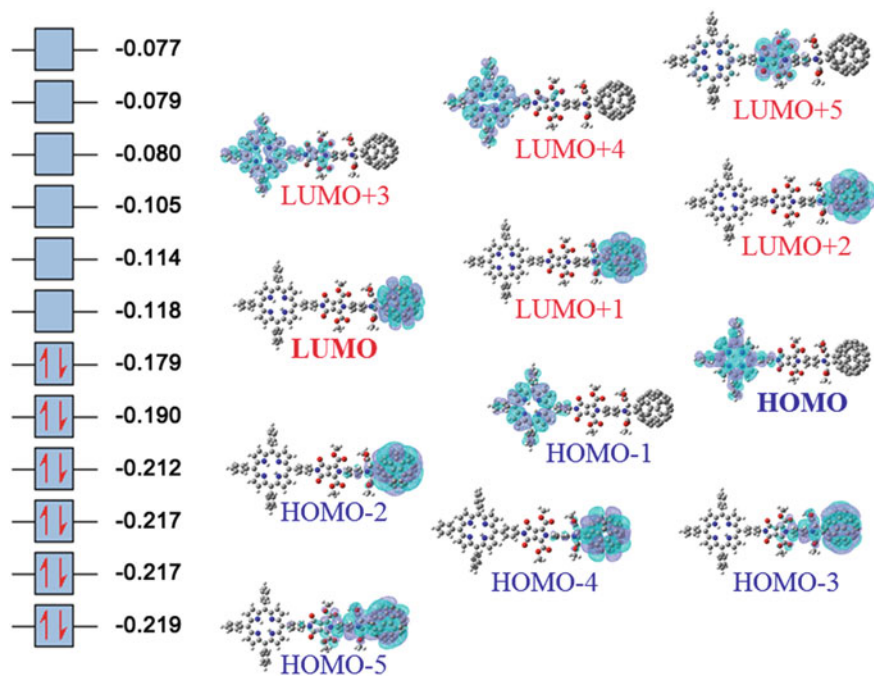

Fig. 22.4 Illustration on local excitation and charge-transfer excitation. Data taken from [22]
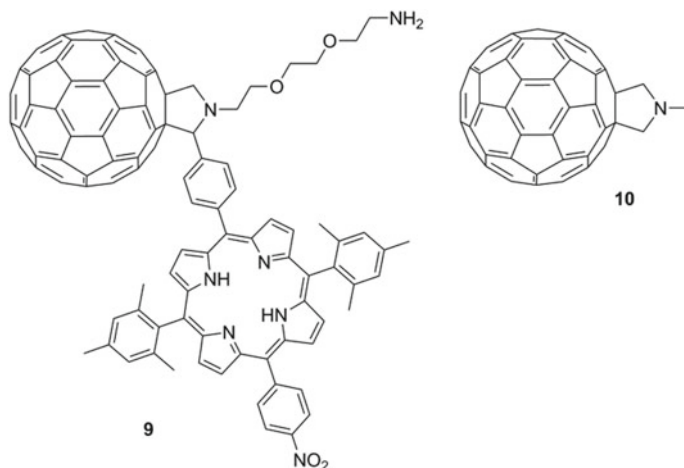
Fig. 22.5 Structural formulae of dyad **9** and pyrrolofullerene **10**

can be found in a porphyrin-fullerene dyads **1a–d** with large interchromophore distance [22]. The substituents in the porphyrin ring show no effect on the energy of fullerene-locally excited states (which is expected) and only a little effect on the energy of porphyrin-locally excited states, but affect dramatically the energy of the charge separated state (Fig. 22.3) [22]. Triplet excited states for both porphyrin and fullerene local excitations have lower energies than the corresponding singlet states, while for charge-separated states no difference was observed for singlet and triplet states [22].

Quantitative prediction of the energy of the charge-separated state for porphyrin-fullerene dyads is a rather complicated task due to the large size of the explored systems. An assessment of the performance of TDDFT and wavefunction based methods is given in the works of Cramariuc et al. for dyads **3** [24] and **4a** [25]. The best match with the experimental value was observed for B3LYP and PBE0 (1.6 eV vs. 1.7–1.8 eV) functionals, other DFT functionals (SVWN, PBE) underestimating the ground state to charge separated state transition energy by ca. 0.7 eV [24, 25] and wavefunction based methods (CCS, CIS(D), CC2) overestimating it by 0.9–1.3 eV [25].

Quantitative performance of TD DFT methods for excited singlet porphyrin states is somewhat better: for dyads **3** [24] and **4a** [25] the calculated excitation energy for the first porphyrin excited singlet state ranged from 1.8 to 2.0 eV (SVWN and PBE functionals) versus the experimental value of 1.89 [24]–1.91 eV [25]. However, for another set of dyads, **1**, TD DFT method showed larger discrepancy with the experimental value: 2.15 eV (B3LYP functional) versus 1.92 eV (experiment) [22]. An interesting observation is a low dependence of the predicted porphyrin excitation energy on the interchromophore distance [24, 25].

Direct assessment of the quantitative performance of TD DFT methods for excited singlet fullerene states is complicated by superimposing of the spectral bands corresponding to the lowest fullerene-based transitions with the spectral bands of much larger intensity corresponding to the porphyrin-based transitions. However, such assessment can be obtained by comparing the computational results obtained for porphyrin-fullerene dyads, where the fullerene core is attached to the molecule as pyrrolofullerene structural fragment, with the results obtained for pyrrolofullerenes not containing porphyrin part. The lowest singlet excited state for *N*-methylpyrrolofullerene (**10**, Fig. 22.5) was calculated to be 1.89 eV (B3LYP) [40], which is 0.11 eV higher than the experimental value of 1.78 eV [41]. The energy of the lowest fullerene singlet excited state in dyads **1** was found to comprise 1.93 eV (B3LYP) [22], just 0.04 eV higher than the energy of the corresponding state in *N*-methylpyrrolofullerene. It is possible to conclude that the attachment of the porphyrin fragment and the linker in dyads **1** has negligible effect on the fullerene localized transitions, which justifies comparison of the energy of the locally excited singlet fullerene state with the experimental values for *N*-methylpyrrolofullerene. So, overestimation of 0.15 eV can be used as the assessment of the performance of TD DFT method (B3LYP) for computing the energy of the excited singlet fullerene state.

22.4 Experimental Observation of Electronically Excited States in Porphyrin-Fullerene Dyads

Population of the electronically excited states in porphyrin-fullerene dyads and the dynamics of their relaxation have been studied in numerous works summarized in the reviews cited in the introduction to the chapter. In this section, the spectral features characteristic for identifying various states are of central interest.

In the studies on photodynamics of the excited states in porphyrin-fullerene dyads, the dyad is excited either in Q band (532, 565 or 590 nm excitation wavelengths were reported) or Soret band (387 [34, 42], 400–403, 425 or 430 nm excitation wavelengths were reported) range (typical Zn-porphyrin spectrum is given on Fig. 22.6). Longer excitation wavelengths excite porphyrin chromophore more selectively. At 387 nm, fullerene chromophore has significant light absorption (ε ca. 7500 $dm^3\ mol^{-1}\ cm^{-1}$ for pyrrolofullerene **10**) [43]. Both porphyrin and fullerene chromophores absorb at 400–403 nm in molar ratio estimated as 4:1 [44]. Pumping at 590 nm allows to achieve the ratio of excitation of porphyrin and fullerene chromophores of 15:1, as it was reported for dyad **3a** [44].

The excitation with 400–430 nm lasers populates porphyrin-excited singlet state corresponding to the Soret band, while excitation by 532 or 590 nm lasers populates lower-lying porphyrin excited singlet state corresponding to Q-bands. The porphyrin excited state corresponding to the Soret band (B-state) is known to undergo fast internal conversion to the vibrationally excited level of the Q state in porphyrins
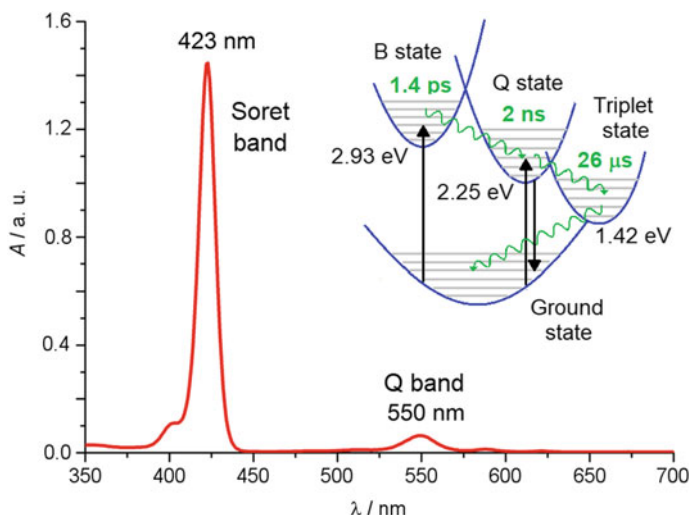
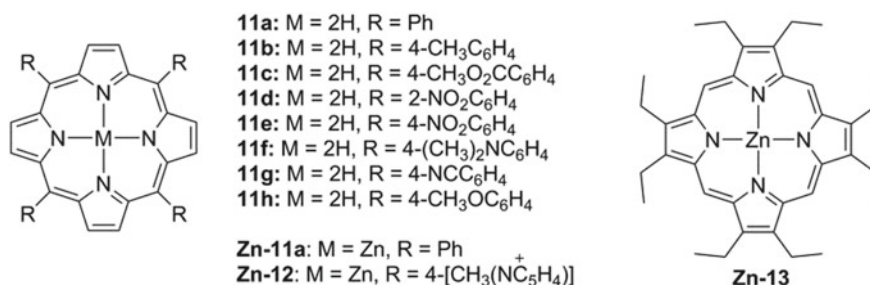**Fig. 22.6** UV-Vis absorption spectrum of porphyrin **Zn-11a** (Fig. 22.7)

11a: M = 2H, R = Ph
11b: M = 2H, R = 4-$CH_3C_6H_4$
11c: M = 2H, R = 4-$CH_3O_2CC_6H_4$
11d: M = 2H, R = 2-$NO_2C_6H_4$
11e: M = 2H, R = 4-$NO_2C_6H_4$
11f: M = 2H, R = 4-$(CH_3)_2NC_6H_4$
11g: M = 2H, R = 4-NCC_6H_4
11h: M = 2H, R = 4-$CH_3OC_6H_4$

Zn-11a: M = Zn, R = Ph
Zn-12: M = Zn, R = 4-$[CH_3(NC_5H_4)]^+$

Fig. 22.7 Structural formulae of porphyrins **11a–h** and **Zn-11a**

(Fig. 22.6). For example, the intrinsic lifetime of the Soret band in benzene solutions comprises 68 fs for *meso*-tetraphenylporphyrin (**11a**, Fig. 22.7) [45] and 1.4 ps for Zn *meso*-tetraphenylporphyrinate (**Zn-11a**) [46]. For porphyrin **11a**, the internal conversion of B-state to Q-state was shown to proceed via a two-channel path: either as a direct conversion of B-state to Q_x-state or via intermediate population of Q_y state [47]. Taking into account rather weak interchromophore interactions in porphyrin-fullerene dyads, similar ultrafast processes are expected to occur in porphyrin-fullerene dyads upon excitation at the Soret band (425/430 nm), making Q state the common intermediate for excitation with both 532 and 425/430 nm lasers.

The Q state in porphyrins undergoes either non-radiative or radiative relaxation to the ground state. The radiative relaxation is seen as fluorescence around 655–690 nm (average wavelength of fluorescence protons, e.g.: 685 nm for porphyrin **11a**) for free-base porphyrins and around 595–635 nm (average wavelength of fluorescence protons, e.g.: 635 nm for porphyrin **Zn-11a**) for Zn porphyrinates [48]. The emis-

sion signal represents two well-resolved peaks, 650 nm/720 nm for porphyrin **11a** (benzene) and 600 nm/650 nm for **Zn-11a** (benzene) being representative example [48]. The Q-state fluorescence lifetime, τ_F, in porphyrins is typically several ns. For example, τ_F comprises 6–16 ns for *meso*-tetraarylporphyrins **11a–h** without heavy atoms [49] and ca. 2 ns for **Zn-11a** [46]. The quantum yield of the fluorescence from Q state of porphyrins is not so high, comprising ca. 0.03–0.15 for porphyrins **11a–h** [49] and 0.02–0.03 for **Zn-11a** [46]. Intersystem crossing to the triplet state of porphyrins constitutes the main deactivation path of the Q-state, the quantum yield of triplet state formation being 0.82 for **11a** and 0.88 for **Zn-11a** [50]. Low temperature (77 K) phosphorescence of **11a** was reported as weak emission (ϕ_P $4 \cdot 10^{-5}$) centered around 865 nm, while more intensive emission (ϕ_P 0.012) with maxima at 780 nm 875 nm for **Zn-11a**, the lifetimes of the triplet state being 6 and 26 ms respectively [50]. Population of the triplet states in porphyrins can be monitored in transient absorption experiment by observing the intensive (ε 10^4 dm^3 mol^{-1} cm^{-1} order of magnitude) triplet-triplet absorption with maximum at ca. 430 and 780 nm for free-base **11a** [51] and ca. 470, 745 and 845 nm for **Zn-11a** [49, 51, 52].

The first excited singlet state of pyrrolofullerenes has a characteristic transient absorption maximum around 900 nm [43] (886 nm for compound **10**) [53] and has the lifetime of ca. 1 ns (1.3 ns for compound **10**) [53]. This state can undergo intersystem crossing populating triplet state with characteristic transient absorption maximum at ca. 700 nm [43] (705 nm [53] for compound **10**).

In porphyrin-fullerene dyads the fluorescence from Q band is significantly quenched, evidenced as the decrease of the quantum yield of the short-living (1–2 ns) $^1P^*$-C_{60} state, analog of the Q-state in porphyrins. In addition to intersystem crossing to long-living (several μs) $^3P^*$-C_{60} state, observed as transient absorption at 470 [44] or 850 nm [32] for Zn-metallated dyads and 450 [22] or 800 nm [32] for free-base dyads (Fig. 22.8), the fluorescence quenching observed is caused by creation of additional relaxation paths upon attaching of the fullerene moiety to the porphyrin. These paths may include either energy transfer, when the energy surplus of $^1P^*$-C_{60} state promotes population of the P-$^1C_{60}^*$ state, or charge transfer, when $^1P^*$-C_{60} state is relaxed to highly polarized charge-separated state. The ratio of these paths depends on the molecular structure of the dyad and on the solvent used in the experiment. In general, polar solvents such as benzonitrile promote formation of the charge-separated state [3, 17, 42, 44], while non-polar solvents like toluene tend to direct the relaxation towards energy transfer path [42].

The energy transfer is usually monitored by observing the emission at 700–750 nm [17, 32, 42, 44], typical of pyrrolofullerenes [54, 55] and benzofullerenes [56] (λ_{max}^{em} 715 nm), which results from the radiative relaxation of P-$^1C_{60}^*$ state to the ground state in pyrrolofullerene- or benzofullerene-based porphyrin-fullerene dyads. The use of emission data for reference pyrrolofullerenes or benzofullerenes for the assignment of the emission at 700–750 nm accords well with the computational studies reporting rather low mutual influence of porphyrin and fullerene electronic systems in dyads. Taking into account non-zero absorption of the fullerene chromophore on the excitation wavelength, the energy transfer should be confirmed by analyzing
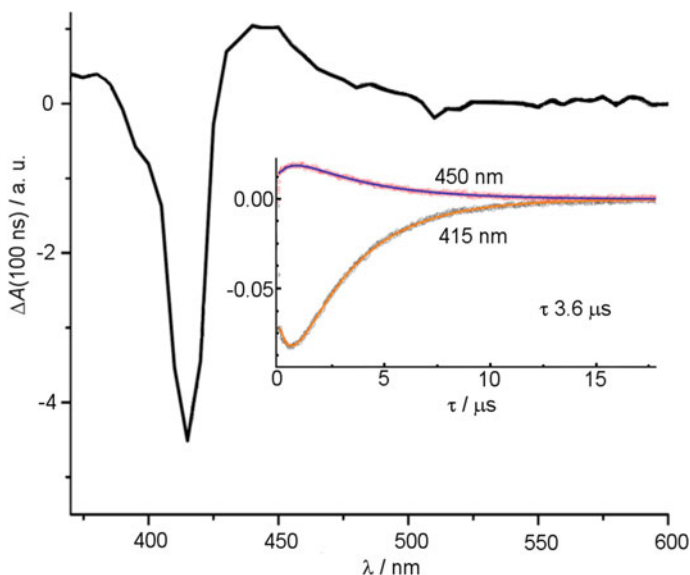
Fig. 22.8 Transient absorption at 450 nm in dyad **1c** due to the formation of $^{3}P^{*}$-C_{60} state. The spectrum recorded in deoxygenated $(CH_2Cl)_2$, λ_{ex} 532 nm, time delay 100 ns. The inset: 450 and 415 ΔA kinetic profiles. Data taken from [22]

excitation spectra for 700 nm emission which should follow the porphyrin rather than pyrrolofullerene absorption pattern [42].

Similar to the case of $^{1}P^{*}$-C_{60} state, population of the P-$^{1}C_{60}^{*}$ state after energy transfer often leads to formation of P-$^{3}C_{60}^{*}$ state via intersystem crossing, which can be monitored by observing fullerene triplet-triplet absorption with maximum at ca. 700 nm in transient absorption experiments on a ns timescale [42].

The charge transfer process in dyads with relatively strong interaction of porphyrin and fullerene is monitored by observing the NIR absorption at ca. 700–800 nm and emission at ca. 750–850 nm [31, 35, 36]. However, in such systems formation of the charge-separated state is accompanied by exciplex formation, which complicates the analysis. In dyads with little or zero interaction of the chromophores in the ground state, monitoring of the charge separated state is performed by observing transient absorption at ca. 900–1050 nm range (transient absorption signals at 900 [31, 34], 920 [44], 1000 [3, 32, 38], 1020 [3, 42] and 1040 nm [39] wavelengths were reported as diagnostic features by different authors) attributed to the local excitation of the fullerene fragment in the charge-separated state and transient absorption at ca. 600–650 nm (transient absorption signals at 600 [32], 620 [32], 630 [34], 640 [3, 38] or 650 nm [31, 39, 44] were reported as diagnostic features by different authors), attributed to the local excitation of the porphyrin fragment in the charge-separated state. The latter marker is usually well observed in Zn-metallated systems but is hard to observe in free-base dyads.

The assignment of the transient absorption at 900–1050 nm to the local excitation of the fullerene fragment in the charge-separated state, conventionally called the absorption of the C_{60}-radical-anion fragment, is based on observation of a similar spectral feature in reduced species of pyrrolofullerenes (1010 nm) [43], methanofullerenes (1040 nm) [43] and pristine fullerene C_{60} (917, 995, 1064 nm) [57]. The 1064 nm absorption in C_{60} radical-anion appears as a sharp signal of large intensity (ε ca. $1.2 \cdot 10^5$ dm^3 mol^{-1} cm^{-1}) and was attributed to symmetry-allowed (0–0) t_{1u}–t_{1g} transition [57].

The assignment of the transient absorption at 600–650 nm to the local excitation of the porphyrin fragment in the charge-separated state, conventionally called the absorption of the Zn-porphyrin radical-cation fragment, is based on observation of a similar spectral feature upon oxidation of Zn-porphyrinates (600–700 nm, **Zn-11a** [58], 700 nm, **Zn-12** [59], 650 nm, **Zn-13** [60]).

Intersystem crossing from the initially formed ^{1}P*-C_{60} state to ^{3}P*-C_{60} state can be also followed by electron transfer generating long-living triplet charge-separated state, which is of special interest for solar energy conversion systems [3].

The lifetimes of the charge-separated states vary from ps to µs timescale, depending on the multiplicity, the structure of the dyad and the solvent used. Close face-to-face alignment of the chromophores results in short-living charge-separated states (ps to 3.5 ns [61, 62]), while large interchromophore distance and face-to-edge alignment tend to favor formation of long-lived charge-separated states [22].

22.5 Conclusion

Computational studies of porphyrin-fullerene covalent dyads predict for them electronic structure which favors charge separation process. In many dyads, a good separation of the chromophores is observed in the ground state, with two sets of orbitals localized each one on a specific chromophore. In particular, HOMO is localized on the porphyrin and LUMO—on the fullerene fragment, which creates the prerequisite for the existence of a highly polarized electronically excited state with HOMO^{1}LUMO^1 configuration. Time-dependent DFT methods predict that localization of the electronic systems of the chromophores in porphyrin-fullerene dyads results in formation of such electronically excited state called charge separated state along with the locally excited states.

The qualitative picture of the electronic states obtained by DFT calculations is supported fairly well with the experimental data: formation of each one of five classes of the electronically excited states was observed by means of either steady-state or transient spectroscopy. The spectral features characteristic of the ground state, charge-separated state, ^{1}P*-C_{60}, ^{3}P*-C_{60}, P-$^1C_{60}$* and P-$^3C_{60}$* states are collected together on Fig. 22.9. Horizontal bars represent spectral ranges where spectroscopic features, either absorption or emission bands, attributed to the ground or a specific electronically excited state have been reported in the literature. The lowest locally excited singlet states, either ^{1}P*-C_{60} or P-$^1C_{60}$* have typically the lifetimes of 1–2 ns,
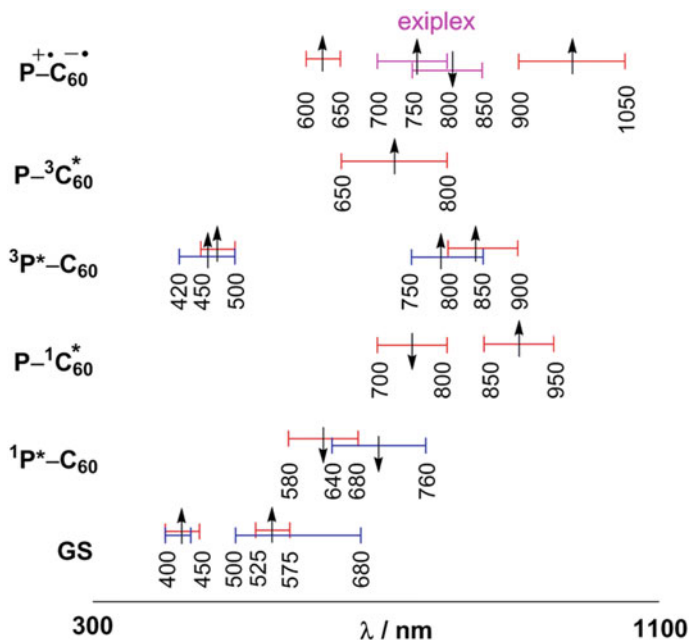
Fig. 22.9 Schematic representation of characteristic spectral features for different types of electronically excited states in porphyrin-fullerene dyads. Arrow up stands for absorption, arrow down stands for emission. Blue bars show spectral ranges characteristic for free-base dyads, in red—for Zn-metallated dyads or common for free base and metallated dyads. Magenta bars show spectral features of exciplex

while locally excited triplet states have the lifetimes up to several μs. The lifetime of the charge-separated state depends strongly on the structure of the compound, the multiplicity of the state and the solvent used in the experiment, varying from ps to μs timescale.

References

1. G.N. Lim, C.O. Obondi, F. D'Souza, Angew. Chem. Int. Ed. **55**, 11517 (2016)
2. N. Martín, Chem. Commun. 2093 (2006)
3. F.D. Souza, O. Ito, Chem. Soc. Rev. **41**, 86 (2012)
4. S. Fukuzumi, K. Ohkubo, T. Suenobu, Acc. Chem. Res. **47**, 1455 (2014)
5. E.N. Durantini, A. Moore, T.A. Moore, D. Gust, Molecules **5**, 529 (2000)
6. M. Fujitsuka, K. Matsumoto, O. Ito, T. Yamashiro, Y. Aso, T. Otsubo, Res. Chem. Intermed. **27**, 73 (2001)

7. H. Imahori, T. Umeyama, K. Kurotobi, Y. Takano, Chem. Commun. **48**, 4032 (2012)
8. M. Vasilopoulou, D.G. Georgiadou, A.M. Douvas, A. Soultati, V. Constantoudis, D. Davazoglou, S. Gardelis, L.C. Palilis, M. Fakis, S. Kennou, T. Lazarides, A.G. Coutsolelos, P.J. Argitis, Mater. Chem. A **2**, 182 (2014)
9. T. Arai, S. Nobukuni, A.S.D. Sandanayaka, O. Ito, J. Phys. Chem. C **113**, 14493 (2009)
10. T. Umeyama, T. Takamatsu, N. Tezuka, Y. Matano, Y. Araki, T. Wada, O. Yoshikawa, T. Sagawa, S. Yoshikawa, H. Imahori, J. Phys. Chem. C **113**, 10798 (2009)
11. H. Imahori, Y. Mori, Y.J. Matano, Photochem. Photobiol. C Photochem. Rev. **4**, 51 (2003)
12. H. Imahori, Y. Sakata, Eur. J. Org. Chem. 2445 (1999)
13. T. Ichiki, Y. Matsuo, E. Nakamura, Chem. Commun. **49**, 279 (2013)
14. Y. Tamura, H. Saeki, J. Hashizume, Y. Okazaki, D. Kuzuhara, M. Suzuki, N. Aratani, H. Yamada, Chem. Commun. **50**, 10379 (2014)
15. N. Kafle, A. Buldum, AIMS Mater. Sci. **4**, 505 (2017)
16. D.M. Guldi, Chem. Soc. Rev. **31**, 22 (2002)
17. H. Imahori, K. Tamaki, H. Yamada, K. Yamada, Carbon **38**, 1599 (2000)
18. H. Lemmetyinen, N. Tkachenko, A. Efimov, M.J. Niemi, Porphyr. Phthalocyanines **13**, 1090 (2009)
19. J. Sukegawa, C. Schubert, X. Zhu, H. Tsuji, D.M. Guldi, E. Nakamura, Nat. Chem. **6**, 899 (2014)
20. O. Ito, Chem. Rec. **17**, 326 (2017)
21. N.J. Agnihotri, Photochem. Photobiol. C Photochem. Rev. **18**, 18 (2014)
22. A.S. Konev, A.F. Khlebnikov, P.I. Prolubnikov, A.S. Mereshchenko, A.V. Povolotskiy, O.V. Levin, A. Hirsch, Chem. Eur. J. **21**, 1237 (2015)
23. M.E. Zandler, F. D'Souza, Comptes Rendus Chim. **9**, 960 (2006)
24. O. Cramariuc, T.I. Hukka, T.T. Rantala, H. Lemmetyinen, J. Phys. Chem. A **110**, 12470 (2006)
25. O. Cramariuc, T.I. Hukka, T.T. Rantala, H. Lemmetyinen, J. Comput. Chem. **30**, 1194 (2009)
26. P.O. Krasnov, Y.M. Milytina, N.S. Eliseeva, Internet Electron. J. Mol. Des. **9**, 20 (2010)
27. T. Karilainen, O. Cramariuc, M. Kuisma, K. Tappura, T.I. Hukka, J. Comput. Chem. **36**, 612 (2015)
28. S. Grimme, J. Comput. Chem. **27**, 1787 (2006)
29. M. Elstner, P. Hobza, T. Frauenheim, S. Suhai, E. Kaxiras, J. Chem. Phys. **114**, 5149 (2001)
30. V. Vehmanen, N.V. Tkachenko, H. Imahori, S. Fukuzumi, H. Lemmetyinen, Spectrochim. Acta A **57**, 2229 (2001)
31. V. Chukharev, N.V. Tkachenko, A. Efimov, D.M. Guldi, A. Hirsch, M. Scheloske, H. Lemmetyinen, J. Phys. Chem. B **108**, 16377 (2004)
32. F. D'Souza, S. Gadde, M.E. Zandler, A. Klykov, M.E. El-Khouly, M. Fujitsuka, O. Ito, J. Phys. Chem. A **106**, 12393 (2002)
33. M.E. El-Khouly, Y. Araki, O. Ito, S. Gadde, A.L. McCarty, P.A. Karr, M.E. Zandler, F. D'Souza, Phys. Chem. Chem. Phys. **7**, 3163 (2005)
34. E. Krokos, C. Schubert, F. Spänig, M. Ruppert, A. Hirsch, D.M. Guldi, Chem. Asian J. **7**, 1451 (2012)
35. H. Imahori, N.V. Tkachenko, V. Vehmanen, K. Tamaki, H. Lemmetyinen, Y. Sakata, S. Fukuzumi, J. Phys. Chem. A **105**, 1750 (2001)
36. V. Chukharev, N.V. Tkachenko, A. Efimov, H. Lemmetyinen, Chem. Phys. Lett. **411**, 501 (2005)
37. A.H. Al-Subi, M. Niemi, J. Ranta, N.V. Tkachenko, H. Lemmetyinen, Chem. Phys. Lett. **531**, 164 (2012)
38. N.V. Tkachenko, H. Lemmetyinen, J. Sonoda, K. Ohkubo, T. Sato, H. Imahori, S. Fukuzumi, J. Phys. Chem. A **107**, 8834 (2003)
39. M.A. Fazio, A. Durandin, N.V. Tkachenko, M. Niemi, H. Lemmetyinen, D.I. Schuster, Chem. Eur. J. **15**, 7698 (2009)
40. I.D. Petsalakis, N. Tagmatarchis, G. Theodorakopoulos, J. Phys. Chem. C **111**, 14139 (2007)
41. M. Maggini, G. Scorrano, M. Prato, J. Am. Chem. Soc. **115**, 9798 (1993)

42. S. Vail, D.I. Schuster, D.M. Guldi, M. Isosomppi, N. Tkachenko, H. Lemmetyinen, A. Palkar, L. Echegoyen, X. Chen, J.Z.H. Zhang, J. Phys. Chem. B **110**, 14155 (2006)
43. D.M. Guldi, M. Prato, Acc. Chem. Res. **33**, 695–703 (2000)
44. H. Imahori, K. Hagiwara, M. Aoki, T. Akiyama, S. Taniguchi, T. Okada, M. Shirakawa, Y. Sakata, J. Am. Chem. Soc. **118**, 11771 (1996)
45. K.Y. Yeon, D. Jeong, S.K. Kim, Chem. Commun. **46**, 5572 (2010)
46. A. Lukaszewicz, J. Karolczak, D. Kowalska, A. Maciejewski, M. Ziolek, R.P. Steer, Chem. Phys. **331**, 359 (2007)
47. S.Y. Kim, T. Joo, J. Phys. Chem. Lett. **6**, 2993 (2015)
48. P.G. Seybold, M. Gouterman, J. Mol. Spectrosc. **31**, 1 (1969)
49. A.J. Harriman, Chem. Soc. Faraday Trans. **2**(77), 1695 (1981)
50. A.J. Harriman, Chem. Soc. Faraday Trans. **2**(76), 1978 (1980)
51. L. Pekkarinen, H. Linschitz, J. Am. Chem. Soc. **82**, 2407 (1960)
52. M. Gouterman, J. Mol. Spectrosc. **6**, 138 (1961)
53. D.M. Guldi, K.D. Asmus, J. Phys. Chem. A **101**, 1472 (1997)
54. F. D'Souza, M.E. Zandler, P.M. Smith, G.R. Deviprasad, A. Klykov, M. Fujitsuka, O. Ito, J. Phys. Chem. A **106**, 649 (2002)
55. D.M. Guldi, M. Maggini, G. Scorrano, M. Prato, J. Am. Chem. Soc. **119**, 974 (1997)
56. J.L. Anderson, Y.Z. An, Y. Rubin, C.S. Foote, J. Am. Chem. Soc. **116**, 9763 (1994)
57. M.A. Greaney, S.M. Gorun, J. Phys. Chem. **95**, 7142 (1991)
58. J. Fajer, D.C. Borg, A. Forman, D. Dolphin, R.H. Felton, J. Am. Chem. Soc. **92**, 3451 (1970)
59. P. Neta, A. Harriman, J. Chem. Soc. Farad. Trans. **81**(2), 123 (1985)
60. J.H. Fuhrhop, D. Mauzerall, J. Am. Chem. Soc. **91**, 4174 (1969)
61. D.I. Schuster, Carbon **38**, 1607 (2000)
62. D.I. Schuster, P. Cheng, P.D. Jarowski, D.M. Guldi, C. Luo, L. Echegoyen, S. Pyo, A.R. Holzwarth, S.E. Braslavsky, R.M. Williams, G. Klihm, J. Am. Chem. Soc. **126**, 7257 (2004)